

Measurement of the Topological Branching Fractions of the τ lepton at LEP

The L3 Collaboration

Abstract

Using data collected with the L3 detector at LEP from 1992 to 1995 on the Z peak, we determine the branching fractions of the τ lepton into one, three and five charged particles to be:

$$\begin{aligned}\mathcal{B}(\tau \rightarrow (1 - prong)) &= 85.274 \pm 0.105 \pm 0.073\%, \\ \mathcal{B}(\tau \rightarrow (3 - prong)) &= 14.556 \pm 0.105 \pm 0.076\%, \\ \mathcal{B}(\tau \rightarrow (5 - prong)) &= 0.170 \pm 0.022 \pm 0.026\%.\end{aligned}$$

The first uncertainties are statistical and the second systematic. The accuracy of these measurements alone is similar to that of the current world average.

Submitted to *Phys. Lett. B*

Introduction

Measurements of the topological branching fractions of the τ lepton and the sum of measurements of the exclusive branching fractions were previously inconsistent. Solving this “one-prong puzzle” motivated many precise determinations of the exclusive τ branching fractions at the permille level [1] but only a few less precise determinations of the topological branching fractions [2] have been performed.

In this letter, we present a new measurement of the topological branching fractions using data collected by the L3 detector at LEP on the Z resonance. These results supersede those of our previous publication [3]. Here we follow the convention that tracks stemming from neutral kaon decays are not accounted for in the topology. Another measurement of the topological τ branching fractions was recently reported in Reference 4.

The measurement entails a selection of $e^+e^- \rightarrow \tau^+\tau^-(\gamma)$ events followed by an event topology reconstruction, which must be precisely understood. The reconstructed topology is influenced by photon conversions, subdetector inefficiencies and resolution limitations. Detailed studies of these effects are performed in order to control the systematic uncertainties to the level of the statistical uncertainties.

Data and Monte Carlo samples

The data used were collected with the L3 detector [5] at LEP from 1992 to 1995 on the Z peak, corresponding to an integrated luminosity of 92.6 pb^{-1} . The most crucial subdetectors for this analysis are: the central tracking system consisting of a silicon microvertex detector (SMD), a time expansion chamber (TEC) and proportional chambers measuring the Z coordinate, the electromagnetic calorimeter composed of Bismuth Germanium Oxide (BGO) crystals, the hadron calorimeter (HCAL) and the muon spectrometer. Detailed studies of the efficiencies of these subdetectors using control samples are performed, yielding precise determinations of the efficiencies.

For efficiency studies, $e^+e^- \rightarrow \tau^+\tau^-(\gamma)$ events are generated with the KORALZ Monte Carlo generator [6]. Background estimations are performed using the following Monte Carlo generators: KORALZ for $e^+e^- \rightarrow \mu^+\mu^-(\gamma)$; BHAGENE [7] for $e^+e^- \rightarrow e^+e^-(\gamma)$; JETSET [8] for $e^+e^- \rightarrow q\bar{q}(\gamma)$; DIAG36 [9] for $e^+e^- \rightarrow e^+e^-\ell^+\ell^-$, where $\ell = e, \mu, \text{ or } \tau$. The Monte Carlo events are simulated in the L3 detector using the GEANT program [10], which takes into account the effects of energy loss, multiple scattering and showering. Furthermore, time dependent detector inefficiencies are considered. These events are reconstructed with the same program as the one used for the data.

Subdetector efficiencies and calibrations

Efficiency studies of the subdetectors are done separately for each year of data taking. As the year-by-year efficiency variations are small, average values are given in the following.

The efficiency of the TEC to measure a track is studied using data samples of Bhabha and dimuon events and muons originating from τ decays. The Bhabha and dimuon samples are selected by requiring two energy deposits in the BGO or two tracks in the muon spectrometer of about the beam energy and back-to-back topology. The muons in τ decays are identified as tracks in the muon chambers pointing to the interaction region. In addition, the energy deposits

in the BGO and HCAL must be consistent with the expectation for a minimum ionising particle (MIP).

A track in the TEC must have at least 25 out of the 62 possible hits, one or more hits in the innermost part of the chamber and to span over more than 40 anode wires radially. Its transverse momentum, p_T , must be larger than 2 GeV. After rejecting tracks in the low resolution region adjacent to the anode, the track finding efficiency is found to be about 96%, almost independent of the track momentum. The double track resolution of the TEC is determined from data [11] to be about $500\mu\text{m}$ and is modeled correspondingly in the detector simulation. As a cross check, the distributions of the azimuthal angle between two adjacent tracks $\Delta\phi$, from data and Monte Carlo are compared in Figure 1 for small values of $\Delta\phi$ and high momentum tracks from 3-prong τ decays. For $\Delta\phi$ larger than 0.005 rad excellent agreement is found. The small discrepancy below 0.005 rad is taken into account as a systematic uncertainty.

The efficiency of the BGO to detect an electromagnetically showering particle is determined using Bhabha events to be about 99.5%. This efficiency is found to be almost independent of the shower energy from studies using $e^+e^- \rightarrow e^+e^-e^+e^-$ events. In order to estimate the efficiency of the BGO to detect a MIP, τ decays into muons are used. A track in the muon spectrometer is required, which points to the interaction region and matches an energy deposit in the HCAL that corresponds to a MIP. From these muons 97% induce a signal in the BGO.

The same technique was used to estimate the HCAL and muon spectrometer efficiencies. Using muons with a track in the TEC, a MIP signal in the BGO and a matched muon spectrometer track, the efficiency of the HCAL to detect such a particle is about 89%. The muon spectrometer efficiency is found to be 74% using τ decays with a track in the TEC and a MIP signature in the BGO and the HCAL.

The subdetector efficiencies obtained from each year are used to correct the Monte Carlo simulation of the detector response for the $e^+e^- \rightarrow \tau^+\tau^-(\gamma)$ and background processes. The energy scales of the subdetectors are calibrated using control data samples [12]. The momentum scale of the central tracker is verified to 0.5% from 1 to 45 GeV. The BGO and the muon spectrometer scale uncertainties are 0.5% at low energies and 0.05% at high energy. The scale uncertainty of the HCAL is 1%.

Study of photon conversions

Photon conversions occurring in the material inside the TEC may cause additional tracks and are studied on data and Monte Carlo for each year independently. A loose selection of $e^+e^- \rightarrow \tau^+\tau^-(\gamma)$ events is made, requiring two low multiplicity jets and the cosine of the polar angle of the event thrust axis $|\cos\theta_{thrust}| < 0.7$. Radiative photons or photons from π^0 decays can convert in the detector. The tracks from the conversion point either to their corresponding cluster in the BGO calorimeter, or to a coalescent cluster including the energy of the two conversion tracks or of the 2 photons in the case of a π^0 decay. Therefore, the p_T measured in the central tracker must be smaller than the transverse energy observed in the electromagnetic calorimeter.

In the case that only one track reaches the TEC, its transverse momentum must be less than 4 GeV. When both tracks are reconstructed, the square of their invariant mass must be less than 0.005 GeV^2 . Taking track pairs which fulfil these requirements, the distance of their vertex to the beam axis, R_v , is calculated. The distribution of R_v is shown in Figure 2 for data from 1994 and Monte Carlo: most of the photon conversions occur at radii between 40 and 90 mm, corresponding to the position of the two cylindrical layers of the SMD. Good agreement of the

simulation of the photon conversion probability inside the TEC with the data is obtained after enlarging the conversion probability by a factor of about 1.6 for data taking periods after the installation of the SMD, to account for additional material not fully considered in the Monte Carlo simulation. The flat background stems mainly from 3-prong hadronic τ decays.

After rejection of identified photon conversions, 0.4% of the τ decays still contain tracks from photon conversions. They are accounted for in the migration efficiencies determined from Monte Carlo.

The effect of tracks scattered back from BGO clusters is investigated. As their momenta are low they are removed by the requirement on the transverse momentum of a track.

Selection of $e^+e^- \rightarrow \tau^+\tau^-(\gamma)$ events

Events of the process $e^+e^- \rightarrow \tau^+\tau^-(\gamma)$ are characterised by two jets with low track and calorimetric cluster multiplicities, where a jet may consist of an isolated electron or muon. To ensure good track measurements only events in the barrel region of the detector are accepted by requiring $|\cos\theta_{thrust}| < 0.7$. The event multiplicity is defined as the sum of the number of tracks in the TEC and the number of neutral calorimetric clusters, without an assigned charged track and with an energy larger than 0.5 GeV. This event multiplicity is required to be less than 10. Each event is divided into two hemispheres with respect to the plane orthogonal to the thrust axis. The main backgrounds arise from two-photon interactions, e^+e^- events and Z decays into two muons. These processes are rejected using information from both hemispheres.

- Two-photon interactions: each hemisphere must contain at least one calorimetric cluster. The sum of the energy deposited in the calorimeters and the muon momenta measured in the muon spectrometer must be larger than 13 GeV.
- e^+e^- events: the total energy deposited in the BGO must be less than 60 GeV. In addition, the energy deposit in each hemisphere must be less than 44 GeV and the acoplanarity angle between the leading tracks of the two hemispheres must be larger than 0.003 rad.
- Z decays into two muons: events with a track in the muon chambers with a momentum larger than 42 GeV are not accepted. Furthermore, events with a muon or a MIP in both hemispheres are rejected.

A sample of 70016 $e^+e^- \rightarrow \tau^+\tau^-(\gamma)$ events is selected. The estimations of the efficiencies and background fractions are done separately for each year. The average selection efficiency for $e^+e^- \rightarrow \tau^+\tau^-(\gamma)$ events inside the barrel, estimated from Monte Carlo, is $78.8 \pm 0.2\%$.

The background from hadronic and other leptonic Z decays and two-photon interactions is estimated from Monte Carlo. As an example, the distribution of the event multiplicity, is shown in Figure 3 for data and a superposition of Monte Carlo from $e^+e^- \rightarrow \tau^+\tau^-(\gamma)$ and background. The background from hadronic Z decays dominates at large values of the multiplicity. After applying a correction factor to the fraction of the hadronic background of 1.05, very good agreement is obtained. The background from Bhabha events is determined using the upper part of the energy distribution measured in the BGO. This is shown in Figure 4 for an event sample with the Bhabha rejection cuts relaxed. The prediction from Bhabha Monte Carlo is scaled by a factor of 1.1 to agree with the data. The background after the final selection is estimated from Bhabha events using this scale factor. The same procedure is applied to estimate the $\mu^+\mu^-$ background. Figure 5 shows the spectrum of muons measured in the muon spectrometer

for data and Monte Carlo after applying a correction factor of 1.1. The background fractions from all sources are listed in Table 1. The cosmic background, estimated from the distribution of the distance of closest approach to the beam position, is found to be negligible.

Determination of the topological branching fractions

The maximum likelihood method is used to determine the topological branching fractions, with likelihood function L defined as:

$$L = \prod_{i=0}^6 P(N_{obs}^i, N_{exp}^i), \quad (1)$$

where P is the Poisson distribution, N_{obs}^i is the number of observed events and N_{exp}^i is the number of expected events with i reconstructed tracks. The latter is:

$$N_{exp}^i = N_{\tau} \sum_{j=1,3,5} \mathcal{B}(j) \varepsilon^{ij} + \sum_k N_{bg}^{ik}, \quad (2)$$

where N_{τ} is the number of τ decays and $\mathcal{B}(j)$ is the branching fraction of j -prong τ decays, $j = 1, 3$ or 5 . The elements of the track detection efficiency matrix, ε^{ij} , are determined from Monte Carlo. The non-diagonal elements represent migrations between the topologies. The number of non-tau background events, N_{bg}^{ik} , obtained from Monte Carlo, is normalised to the data luminosity. The index k runs over all background sources.

The efficiency matrix of the track reconstruction is shown in Table 2, indicating the numbers of reconstructed tracks for τ decays to 1, 3 and 5 charged particles. Tracks arising from neutral kaon decays are not accounted for in the topology. Table 3 shows the number of observed τ decays in the different topologies and the estimated background. In the fit the constraint $\mathcal{B}(1) + \mathcal{B}(3) + \mathcal{B}(5) = 1$ is applied and the sum of N_{exp}^i is constrained to the number of observed τ decays. The following results are obtained:

$$\begin{aligned} \mathcal{B}(1 - prong) &= 85.274 \pm 0.105\%, \\ \mathcal{B}(3 - prong) &= 14.556 \pm 0.105\%, \\ \mathcal{B}(5 - prong) &= 0.170 \pm 0.022\%, \end{aligned}$$

where the uncertainty is statistical only. The $\chi^2/\text{d.o.f.}$ is 5.7/4. The correlation coefficients are given in Table 4.

In Figures 6 and 7 the number of observed τ decays is shown as a function of the charged track multiplicity in linear and logarithmic scale, respectively. Also shown are the Monte Carlo predictions, using the fitted branching fractions, and the background.

Systematic uncertainties

The criteria to suppress the different background sources are varied within reasonable ranges and the changes in the topological branching fractions are taken as systematic uncertainties. The uncertainty on the cross section of $e^+e^- \rightarrow \text{hadrons}$ [13] and the scale factor applied to the Monte Carlo normalisation are considered. The cross section uncertainties on e^+e^- and $\mu^+\mu^-$ final states and two-photon interactions have negligible effects on the branching fractions. The

background uncertainties from e^+e^- and $\mu^+\mu^-$ final states are obtained from the statistical uncertainty of 1% on the scale factors applied to the Monte Carlo distributions shown in Figures 4 and 5. The systematic uncertainty due to track efficiency is obtained by varying this quantity within its statistical uncertainty of 0.25%. Furthermore, the track definition criteria are changed within reasonable ranges. The uncertainty from double track resolution is estimated by reweighting the $\Delta\phi$ distribution of Figure 1 forcing agreement between data and Monte Carlo in the low $\Delta\phi$ region. The effects on the branching fractions are taken as systematic uncertainties.

The systematic uncertainty due to photon conversions is obtained from the statistical uncertainty of 10% on the photon conversion probability correction factor and from variations of conversion identification criteria.

The uncertainty from Monte Carlo statistics is included as statistical uncertainties on the efficiency matrix in Table 1. The resulting variations on the branching fractions are taken as systematic uncertainties. Effects from the energy scale uncertainties of the subdetectors are negligible. A summary of the systematic uncertainties is provided in Table 5.

After combination of the systematic uncertainties the results for the branching fractions of the τ lepton decays into one, three and five charged particle final states are:

$$\begin{aligned}\mathcal{B}(\tau \rightarrow (1 - prong)) &= 85.274 \pm 0.105 \pm 0.073\%, \\ \mathcal{B}(\tau \rightarrow (3 - prong)) &= 14.556 \pm 0.105 \pm 0.076\%, \\ \mathcal{B}(\tau \rightarrow (5 - prong)) &= 0.170 \pm 0.022 \pm 0.026\%,\end{aligned}$$

where the first uncertainty is statistical and the second is systematic. These new results are in agreement with a recent measurement with the full LEP statistics [4] and with the current world averages [1].

Acknowledgements

We wish to express our gratitude to the CERN accelerator division for the excellent performance of the LEP machine. We acknowledge the contributions of engineers and technicians who have participated in the construction and maintenance of this experiment.

References

- [1] D.E. Groom *et al.*, Eur. Phys. J. **C 15** (2000) 1
- [2] ARGUS Collab., H. Albrecht *et al.*, Z. Phys. **C 53** (1992) 367; OPAL Collab., P.D. Acton *et al.*, Phys. Lett. **B 288** (1992) 373; CLEO Collab., R. Balest *et al.*, Phys. Rev. Lett. **75** (1995) 3809; OPAL Collab., R. Akers *et al.*, Z. Phys. **C 68** (1995) 555
- [3] L3 Collab., B. Adeva *et al.*, Phys. Lett. **B 265** (1991) 451
- [4] DELPHI Coll., P. Abreu *et al.*, Preprint CERN-EP/2001-030
- [5] L3 Collab., B. Adeva *et al.*, Nucl. Instr. Meth. **A 289** (1990) 35; J.A. Bakken *et al.*, Nucl. Instr. Meth. **A 275** (1989) 81; O. Adriani *et al.*, Nucl. Instr. Meth. **A 302** (1991) 53; B. Adeva *et al.*, Nucl. Instr. Meth. **A 323** (1992) 109; K. Deiters *et al.*, Nucl. Instr. Meth. **A 323** (1992) 162; M. Chemarin *et al.*, Nucl. Instr. Meth. **A 349** (1994) 345; M. Acciarri *et al.*, Nucl. Instr. Meth. **A 351** (1994) 300
- [6] S. Jadach, B.F.L. Ward and Z. Wąs, Comp. Phys. Comm. **79** (1994) 503
- [7] J.H. Field, Phys. Lett. **B 323** (1994) 432; J.H. Field and T. Riemann, Comp. Phys. Comm **94** (1996) 53
- [8] T. Sjöstrand, Comp. Phys. Comm. **39** (1986) 347; T. Sjöstrand and M. Bengtsson, Comp. Phys. Comm. **43** (1987) 367
- [9] F.A. Berends, P.H. Daverfeldt and R. Kleiss, Nucl. Phys. **B 253** (1985) 441
- [10] R. Brun *et al.*, Preprint CERN DD/EE/84-1 (1984), revised September 1987. The GHEISHA program (H. Fesefeldt, RWTH Aachen Report PITHA 85/02, 1985) is used to simulate hadronic interactions
- [11] F. Beissel *et al.*, Nucl. Inst. and Meth. **A 332** (1993) 33
- [12] L3 Collab., M. Acciarri *et al.*, Phys. Lett. **B 429** (1998) 387
- [13] L3 Collab., M. Acciarri *et al.*, Eur. Phys. J. **C 16** (2000) 1

The L3 Collaboration:

P.Achard,²⁰ O.Adriani,¹⁷ M.Aguilar-Benitez,²⁴ J.Alcaraz,^{24,18} G.Alemanni,²² J.Allaby,¹⁸ A.Aloisio,²⁸ M.G.Alvigi,²⁸ H.Anderhub,⁴⁷ V.P.Andreev,^{6,33} F.Anselmo,⁹ A.Arefiev,²⁷ T.Azmoon,³ T.Aziz,^{10,18} M.Baarmand,²⁵ P.Bagnaia,³⁸ A.Bajo,²⁴ G.Baksay,¹⁶ L.Baksay,²⁵ S.V.Baldew,² S.Banerjee,¹⁰ Sw.Banerjee,⁴ A.Barczyk,^{47,45} R.Barillère,¹⁸ P.Bartolini,²² M.Basile,⁹ N.Batalova,⁴⁴ R.Battiston,³² A.Bay,²² F.Becattini,¹⁷ U.Becker,¹⁴ F.Behner,⁴⁷ L.Bellucci,¹⁷ R.Berbeco,³ J.Berdugo,²⁴ P.Berges,¹⁴ B.Bertucci,³² B.L.Betev,⁴⁷ M.Biasini,³² M.Biglietti,²⁸ A.Biland,⁴⁷ J.J.Blaising,⁴ S.C.Blyth,³⁴ G.J.Bobbink,² A.Böhm,¹ L.Boldizsar,¹³ B.Borgia,³⁸ D.Bourilkov,⁴⁷ M.Bourquin,²⁰ S.Braccini,²⁰ J.G.Branson,⁴⁰ F.Brochu,⁴ A.Buijs,⁴³ J.D.Burger,¹⁴ W.J.Burger,³² X.D.Cai,¹⁴ M.Capell,¹⁴ G.Cara Romeo,⁹ G.Carlino,²⁸ A.Cartacci,¹⁷ J.Casaus,²⁴ F.Cavallari,³⁸ N.Cavallo,³⁵ C.Cecchi,³² M.Cerrada,²⁴ M.Chamizo,²⁰ Y.H.Chang,⁴⁹ M.Chemarin,²³ A.Chen,⁴⁹ G.Chen,⁷ G.M.Chen,⁷ H.F.Chen,²¹ H.S.Chen,⁷ G.Chiefari,²⁸ L.Cifarelli,³⁹ F.Cindolo,⁹ I.Clare,¹⁴ R.Clare,³⁷ G.Coignet,⁴ A.P.Colijn,² N.Colino,²⁴ S.Costantini,³⁸ B.de la Cruz,²⁴ S.Cucciarelli,³² T.S.Dai,¹⁴ J.A.van Dalen,³⁰ R.de Asmundis,²⁸ P.Déglon,²⁰ J.M.Debreczeni,¹³ A.Degré,⁴ K.Deiters,⁴⁵ D.della Volpe,²⁸ E.Delmeire,²⁰ P.Denes,³⁶ F.DeNotaristefani,³⁸ A.De Salvo,⁴⁷ M.Diemoz,³⁸ M.Dierckxsens,² D.van Dierendonck,² C.Dionisi,³⁸ M.Dittmar,^{47,18} A.Doria,²⁸ M.T.Dova,^{11,5} D.Duchesneau,⁴ P.Duinker,² B.Echenard,²⁰ A.Eline,¹⁸ H.El Mamouni,²³ A.Engler,³⁴ F.J.Eppling,¹⁴ A.Ewers,¹ P.Extermann,²⁰ M.A.Falagan,²⁴ S.Falciano,³⁸ A.Favara,³¹ J.Fay,²³ O.Fedin,³³ M.Felcini,⁴⁷ T.Ferguson,³⁴ H.Fesefeldt,¹ E.Fiandrini,³² J.H.Field,²⁰ F.Filthaut,³⁰ P.H.Fisher,¹⁴ W.Fisher,³⁶ I.Fisk,⁴⁰ G.Forconi,¹⁴ K.Freudenreich,⁴⁷ C.Furetta,²⁶ Yu.Galaktionov,^{27,14} S.N.Ganguli,¹⁰ P.Garcia-Abia,^{5,18} M.Gataullin,³¹ S.Gentile,³⁸ S.Giagu,³⁸ Z.F.Gong,²¹ G.Grenier,²³ O.Grimm,⁴⁷ M.W.Gruenewald,^{8,1} M.Guida,³⁹ R.van Gulik,² V.K.Gupta,³⁶ A.Gurtu,¹⁰ L.J.Gutay,⁴⁴ D.Haas,⁵ D.Hatzifotiadiou,⁹ T.Hebbeker,^{8,1} A.Hervé,¹⁸ J.Hirschfelder,³⁴ H.Hofer,⁴⁷ G.Holzner,⁴⁷ S.R.Hou,⁴⁹ Y.Hu,³⁰ B.N.Jin,⁷ L.W.Jones,³ P.de Jong,² I.Josa-Mutuberría,²⁴ D.Käfer,¹⁵ M.Kaur,¹⁵ M.N.Kienzle-Focacci,²⁰ J.K.Kim,⁴² J.Kirkby,¹⁸ W.Kittel,³⁰ A.Klimentov,^{14,27} A.C.König,³⁰ M.Kopal,⁴⁴ V.Koutsenko,^{14,27} M.Kräber,⁴⁷ R.W.Kraemer,³⁴ A.Krenz,¹ A.Krüger,⁴⁶ A.Kunin,^{14,27} P.Lacetre,^{46,5} P.Ladron de Guevara,²⁴ I.Laktineh,²³ G.Landi,¹⁷ M.Lebeau,¹⁸ A.Lebedev,¹⁴ P.Lebun,²³ P.Lecomte,⁴⁷ P.Lecoq,¹⁸ P.Le Coultre,⁴⁷ H.J.Lee,⁸ J.M.Le Goff,¹⁸ R.Leiste,⁴⁶ P.Levtchenko,³³ C.Li,²¹ S.Likhoded,⁴⁶ C.H.Lin,⁴⁹ W.T.Lin,⁴⁹ F.L.Linde,² L.Lista,²⁸ Z.A.Liu,⁷ W.Lohmann,⁴⁶ E.Longo,³⁸ Y.S.Lu,⁷ K.Lübelsmeyer,¹ C.Luci,³⁸ D.Luckey,¹⁴ L.Luminari,³⁸ W.Lustermann,⁴⁷ W.G.Ma,²¹ L.Malgeri,²⁰ A.Malinin,²⁷ C.Maña,²⁴ D.Mangeol,³⁰ J.Mans,³⁶ J.P.Martin,²³ F.Marzano,³⁸ K.Mazumdar,¹⁰ R.R.McNeil,⁶ S.Mele,^{18,28} L.Merola,²⁸ M.Meschini,¹⁷ W.J.Metzger,³⁰ A.Mihul,¹² H.Milcent,¹⁸ G.Mirabelli,³⁸ J.Mnich,¹ G.B.Mohanty,¹⁰ R.Moore,³ G.S.Muanza,²³ A.J.M.Muijs,² B.Musicar,⁴⁰ M.Musy,³⁸ S.Nagy,¹⁶ M.Napolitano,²⁸ F.Nessi-Tedaldi,⁴⁷ H.Newman,³¹ T.Niessen,¹ A.Nisati,³⁸ H.Nowak,⁴⁶ R.Ofierzynski,⁴⁷ G.Organtini,³⁸ C.Palomares,¹⁸ D.Pandoulas,¹ P.Paolucci,²⁸ R.Paramatti,³⁸ G.Passaleva,¹⁷ S.Patricelli,²⁸ T.Paul,¹¹ M.Pauluzzi,³² C.Paus,¹⁴ F.Pauss,⁴⁷ M.Pedace,³⁸ S.Pensotti,²⁶ D.Perret-Gallix,⁴ B.Petersen,³⁰ D.Piccolo,²⁸ F.Pierella,⁹ P.A.Piroué,³⁶ E.Pistolesi,²⁶ V.Plyaskin,²⁷ M.Pohl,²⁰ V.Pojidaev,¹⁷ H.Postema,¹⁴ J.Pothier,¹⁸ D.O.Prokofiev,⁴⁴ D.Prokofiev,³³ J.Quartieri,³⁹ G.Rahal-Callot,⁴⁷ M.A.Rahaman,¹⁰ P.Raics,¹⁶ N.Raja,¹⁰ R.Ramelli,⁴⁷ P.G.Rancoita,²⁶ R.Ranieri,¹⁷ A.Raspereza,⁴⁶ P.Razis,²⁹ D.Ren,⁴⁷ M.Rescigno,³⁸ S.Reucroft,¹¹ S.Riemann,⁴⁶ K.Riles,³ B.P.Roe,³ L.Romero,²⁴ A.Rosca,⁸ S.Rosier-Lees,⁴ S.Roth,¹ C.Rosenbleck,¹ B.Roux,³⁰ J.A.Rubio,¹⁸ G.Ruggiero,¹⁷ H.Rykaczewski,⁴⁷ A.Sakharov,⁴⁷ S.Saremi,⁶ S.Sarkar,³⁸ J.Salicio,¹⁸ E.Sanchez,²⁴ M.P.Sanders,³⁰ C.Schäfer,¹⁸ V.Schegelsky,³³ S.Schmidt-Kaerst,¹ D.Schmitz,¹ H.Schopper,⁴⁸ D.J.Schotanus,³⁰ G.Schwering,¹ C.Sciacca,²⁸ L.Servoli,³² S.Shevchenko,³¹ N.Shivarov,⁴¹ V.Shoutko,^{27,14} E.Shumilov,²⁷ A.Shvorob,³¹ T.Siedenburger,¹ D.Son,⁴² P.Spillantini,¹⁷ M.Steuer,¹⁴ D.P.Stickland,³⁶ B.Stoyanov,⁴¹ A.Straessner,¹⁸ K.Sudhakar,¹⁰ G.Sultanov,⁴¹ L.Z.Sun,²¹ S.Sushkov,⁸ H.Suter,⁴⁷ J.D.Swain,¹¹ Z.Szillasi,^{25,¶} X.W.Tang,⁷ P.Tarjan,¹⁶ L.Tauscher,⁵ L.Taylor,¹¹ B.Tellili,²³ D.Teyssier,²³ C.Timmermans,³⁰ Samuel C.C.Ting,¹⁴ S.M.Ting,¹⁴ S.C.Tonwar,^{10,18} J.Tóth,¹³ C.Tully,³⁶ K.L.Tung,⁷ Y.Uchida,¹⁴ J.Ulbricht,⁴⁷ E.Valente,³⁸ R.T.Van de Walle,³⁰ V.Veszpremi,²⁵ G.Vesztergombi,¹³ I.Vetlitsky,²⁷ D.Vicinanza,³⁹ G.Viertel,⁴⁷ S.Villa,³⁷ M.Vivargent,⁴ S.Vlachos,⁵ I.Vodopianov,³³ H.Vogel,³⁴ H.Vogt,⁴⁶ I.Vorobiev,³⁴²⁷ A.A.Vorobyov,³³ M.Wadhwa,⁵ W.Wallraff,¹ M.Wang,¹⁴ X.L.Wang,²¹ Z.M.Wang,²¹ M.Weber,¹ P.Wienemann,¹ H.Wilkens,³⁰ S.X.Wu,¹⁴ S.Wynhoff,³⁶ L.Xia,³¹ Z.Z.Xu,²¹ J.Yamamoto,³ B.Z.Yang,²¹ C.G.Yang,⁷ H.J.Yang,³ M.Yang,⁷ S.C.Yeh,⁵⁰ An.Zalite,³³ Yu.Zalite,³³ Z.P.Zhang,²¹ J.Zhao,²¹ G.Y.Zhu,⁷ R.Y.Zhu,³¹ H.L.Zhuang,⁷ A.Zichichi,^{9,18,19} F.Ziegler,⁴⁶ G.Zilizi,^{25,¶} B.Zimmermann,⁴⁷ M.Zöller.¹

- 1 I. Physikalisches Institut, RWTH, D-52056 Aachen, FRG[§]
 - III. Physikalisches Institut, RWTH, D-52056 Aachen, FRG[§]
 - 2 National Institute for High Energy Physics, NIKHEF, and University of Amsterdam, NL-1009 DB Amsterdam, The Netherlands
 - 3 University of Michigan, Ann Arbor, MI 48109, USA
 - 4 Laboratoire d'Annecy-le-Vieux de Physique des Particules, LAPP,IN2P3-CNRS, BP 110, F-74941 Annecy-le-Vieux CEDEX, France
 - 5 Institute of Physics, University of Basel, CH-4056 Basel, Switzerland
 - 6 Louisiana State University, Baton Rouge, LA 70803, USA
 - 7 Institute of High Energy Physics, IHEP, 100039 Beijing, China[△]
 - 8 Humboldt University, D-10099 Berlin, FRG[§]
 - 9 University of Bologna and INFN-Sezione di Bologna, I-40126 Bologna, Italy
 - 10 Tata Institute of Fundamental Research, Mumbai (Bombay) 400 005, India
 - 11 Northeastern University, Boston, MA 02115, USA
 - 12 Institute of Atomic Physics and University of Bucharest, R-76900 Bucharest, Romania
 - 13 Central Research Institute for Physics of the Hungarian Academy of Sciences, H-1525 Budapest 114, Hungary[‡]
 - 14 Massachusetts Institute of Technology, Cambridge, MA 02139, USA
 - 15 Panjab University, Chandigarh 160 014, India.
 - 16 KLTE-ATOMKI, H-4010 Debrecen, Hungary[¶]
 - 17 INFN Sezione di Firenze and University of Florence, I-50125 Florence, Italy
 - 18 European Laboratory for Particle Physics, CERN, CH-1211 Geneva 23, Switzerland
 - 19 World Laboratory, FBLJA Project, CH-1211 Geneva 23, Switzerland
 - 20 University of Geneva, CH-1211 Geneva 4, Switzerland
 - 21 Chinese University of Science and Technology, USTC, Hefei, Anhui 230 029, China[△]
 - 22 University of Lausanne, CH-1015 Lausanne, Switzerland
 - 23 Institut de Physique Nucléaire de Lyon, IN2P3-CNRS, Université Claude Bernard, F-69622 Villeurbanne, France
 - 24 Centro de Investigaciones Energéticas, Medioambientales y Tecnológicas, CIEMAT, E-28040 Madrid, Spain[‡]
 - 25 Florida Institute of Technology, Melbourne, FL 32901, USA
 - 26 INFN-Sezione di Milano, I-20133 Milan, Italy
 - 27 Institute of Theoretical and Experimental Physics, ITEP, Moscow, Russia
 - 28 INFN-Sezione di Napoli and University of Naples, I-80125 Naples, Italy
 - 29 Department of Physics, University of Cyprus, Nicosia, Cyprus
 - 30 University of Nijmegen and NIKHEF, NL-6525 ED Nijmegen, The Netherlands
 - 31 California Institute of Technology, Pasadena, CA 91125, USA
 - 32 INFN-Sezione di Perugia and Università Degli Studi di Perugia, I-06100 Perugia, Italy
 - 33 Nuclear Physics Institute, St. Petersburg, Russia
 - 34 Carnegie Mellon University, Pittsburgh, PA 15213, USA
 - 35 INFN-Sezione di Napoli and University of Potenza, I-85100 Potenza, Italy
 - 36 Princeton University, Princeton, NJ 08544, USA
 - 37 University of California, Riverside, CA 92521, USA
 - 38 INFN-Sezione di Roma and University of Rome, "La Sapienza", I-00185 Rome, Italy
 - 39 University and INFN, Salerno, I-84100 Salerno, Italy
 - 40 University of California, San Diego, CA 92093, USA
 - 41 Bulgarian Academy of Sciences, Central Lab. of Mechatronics and Instrumentation, BU-1113 Sofia, Bulgaria
 - 42 The Center for High Energy Physics, Kyungpook National University, 702-701 Taegu, Republic of Korea
 - 43 Utrecht University and NIKHEF, NL-3584 CB Utrecht, The Netherlands
 - 44 Purdue University, West Lafayette, IN 47907, USA
 - 45 Paul Scherrer Institut, PSI, CH-5232 Villigen, Switzerland
 - 46 DESY, D-15738 Zeuthen, FRG
 - 47 Eidgenössische Technische Hochschule, ETH Zürich, CH-8093 Zürich, Switzerland
 - 48 University of Hamburg, D-22761 Hamburg, FRG
 - 49 National Central University, Chung-Li, Taiwan, China
 - 50 Department of Physics, National Tsing Hua University, Taiwan, China
- § Supported by the German Bundesministerium für Bildung, Wissenschaft, Forschung und Technologie
- ‡ Supported by the Hungarian OTKA fund under contract numbers T019181, F023259 and T024011.
- ¶ Also supported by the Hungarian OTKA fund under contract number T026178.
- ‡ Supported also by the Comisión Interministerial de Ciencia y Tecnología.
- ‡ Also supported by CONICET and Universidad Nacional de La Plata, CC 67, 1900 La Plata, Argentina.
- ‡ Also supported by Deutscher akademischer Austauschdienst.
- △ Supported by the National Natural Science Foundation of China.

Background source	Fraction [%]
$Z \rightarrow \text{hadrons}$	1.59
Two-photon interactions	0.16
$e^+e^- \rightarrow e^+e^-(\gamma)$	0.16
$e^+e^- \rightarrow \mu^+\mu^-(\gamma)$	0.68

Table 1: The background fractions from the different sources in the $e^+e^- \rightarrow \tau^+\tau^-(\gamma)$ event sample.

N_{rec}	N_{gen}		
	1	3	5
0	7.58 ± 0.02	0.78 ± 0.01	0.84 ± 0.15
1	70.18 ± 0.05	6.88 ± 0.04	3.58 ± 0.30
2	0.33 ± 0.01	26.89 ± 0.07	9.55 ± 0.50
3	0.16 ± 0.01	47.05 ± 0.09	20.50 ± 0.73
4	<0.01	0.21 ± 0.01	24.38 ± 0.79
5	<0.01	0.05 ± 0.01	14.88 ± 0.63
6	<0.01	<0.01	<0.01

Table 2: The efficiency matrix of track reconstruction in percent. N_{gen} denotes the number of charged tracks of the τ decay before detector simulation and N_{rec} the number of tracks after the reconstruction.

N_{rec}	0	1	2	3	4	5	6
Data	11935	107283	8166	12378	216	53	1
Background [%]	3.7	1.9	9.7	2.5	33.8	7.6	0

Table 3: The number of τ decays observed in the different topologies and background estimated by Monte Carlo.

Source	$\mathcal{B}(1 - prong)$	$\mathcal{B}(3 - prong)$	$\mathcal{B}(5 - prong)$
$\mathcal{B}(1 - prong)$	1.0	-0.978	-0.082
$\mathcal{B}(3 - prong)$		1.0	-0.127
$\mathcal{B}(5 - prong)$			1.0

Table 4: The correlation coefficients obtained from a fit of the topological branching fractions.

Source	$\mathcal{B}(1 - prong)$	$\mathcal{B}(3 - prong)$	$\mathcal{B}(5 - prong)$
Z \rightarrow hadrons	0.048	0.052	0.024
$e^+e^- \rightarrow e^+e^-(\gamma)$	0.010	0.010	0.001
$e^+e^- \rightarrow \mu^+\mu^-(\gamma)$	0.010	0.010	0.001
Two-photon interactions	0.011	0.011	0.001
Track definition	0.035	0.035	0.003
Double track resolution	0.012	0.012	0.001
Photon conversions	0.017	0.017	0.004
Monte Carlo statistics	0.032	0.032	0.007
Total	0.073	0.076	0.026

Table 5: Systematic uncertainties in % on the branching fractions resulting from the listed sources and their combined values.

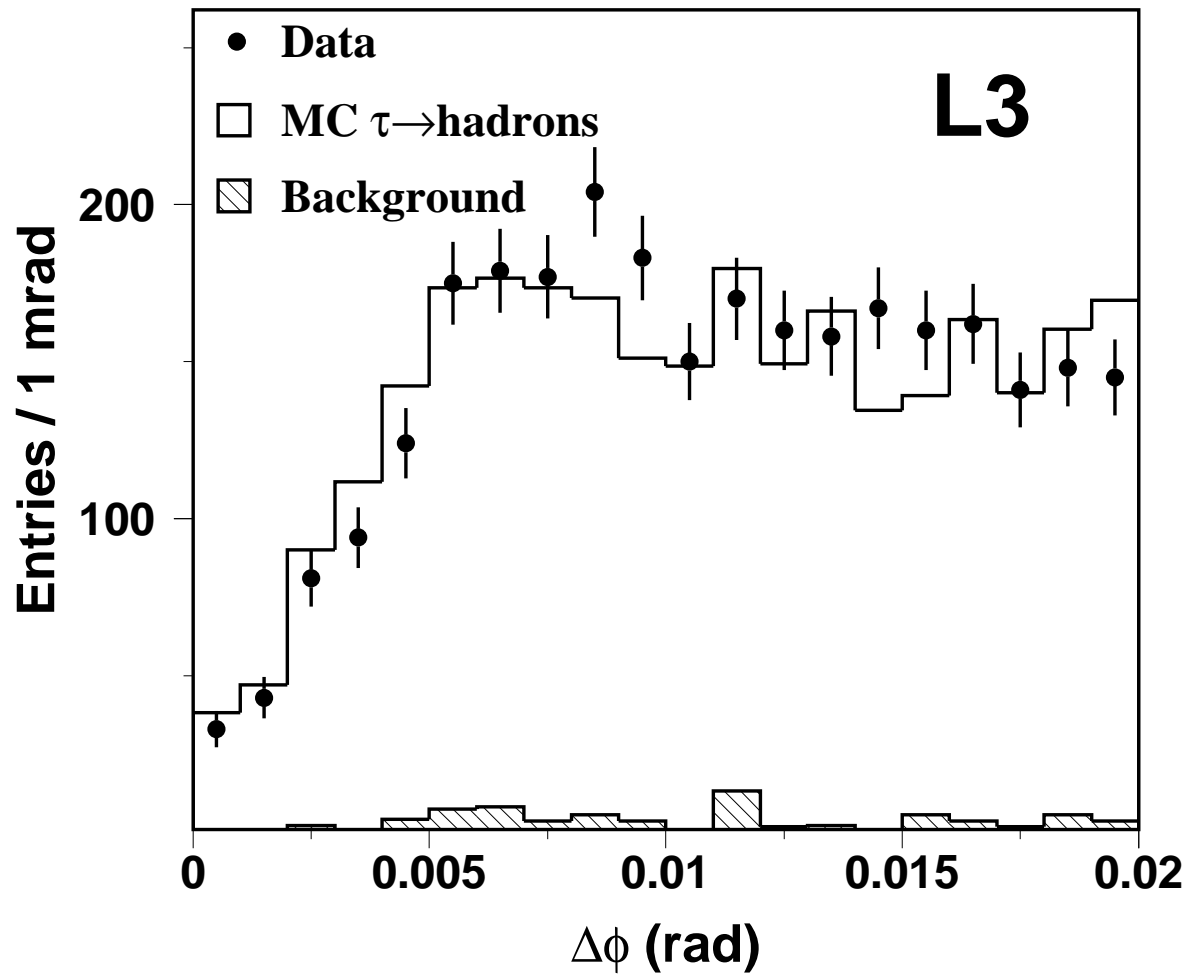


Figure 1: Distribution of the azimuthal angle between two adjacent tracks $\Delta\phi$, where the tracks must have a transverse momentum larger than 10 GeV.

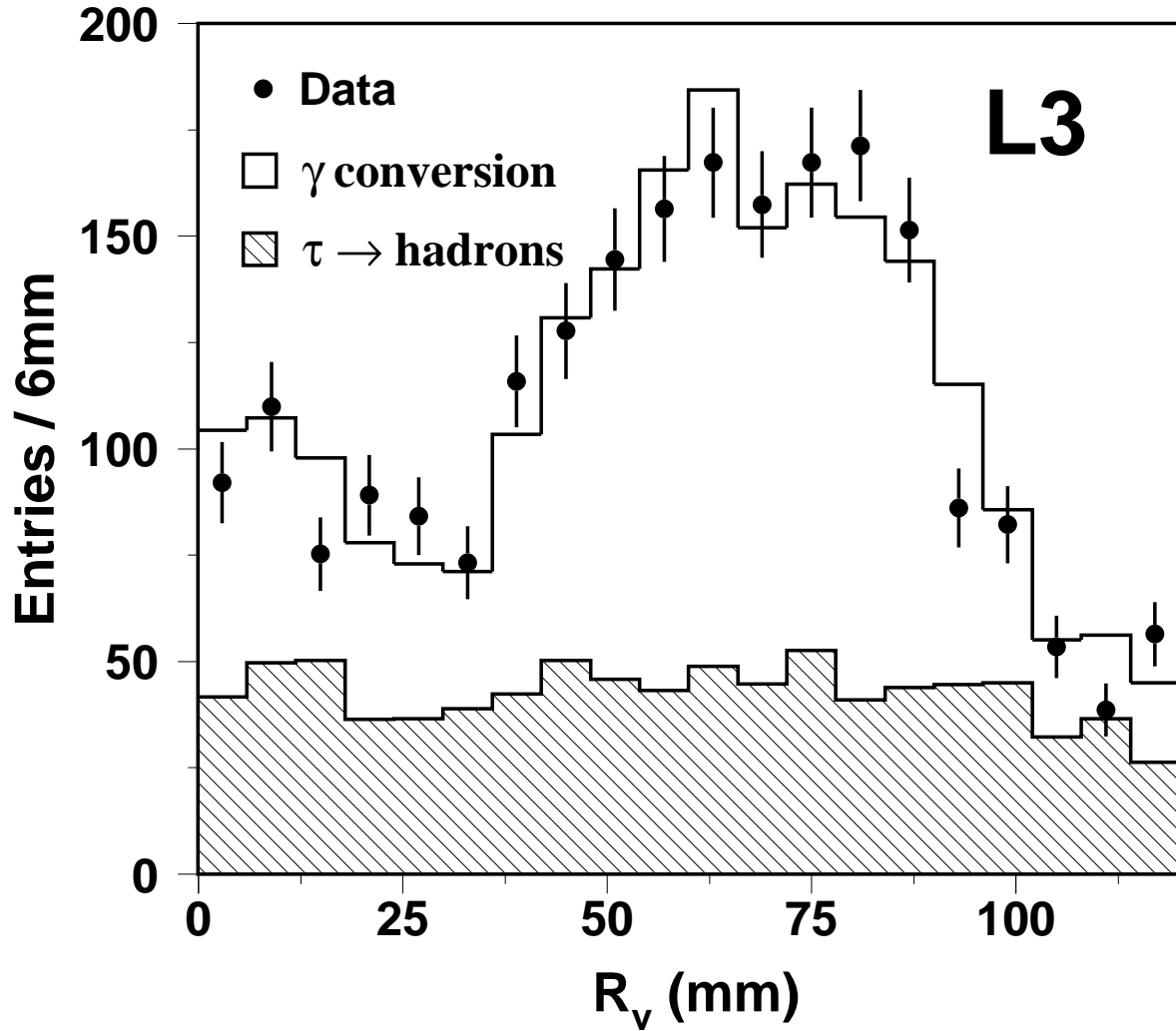


Figure 2: Distribution of the radial distance from the beam axis, R_v , of vertices reconstructed using photon conversion tracks. The flat hatched distribution stems from track pairs of hadronic τ decays.

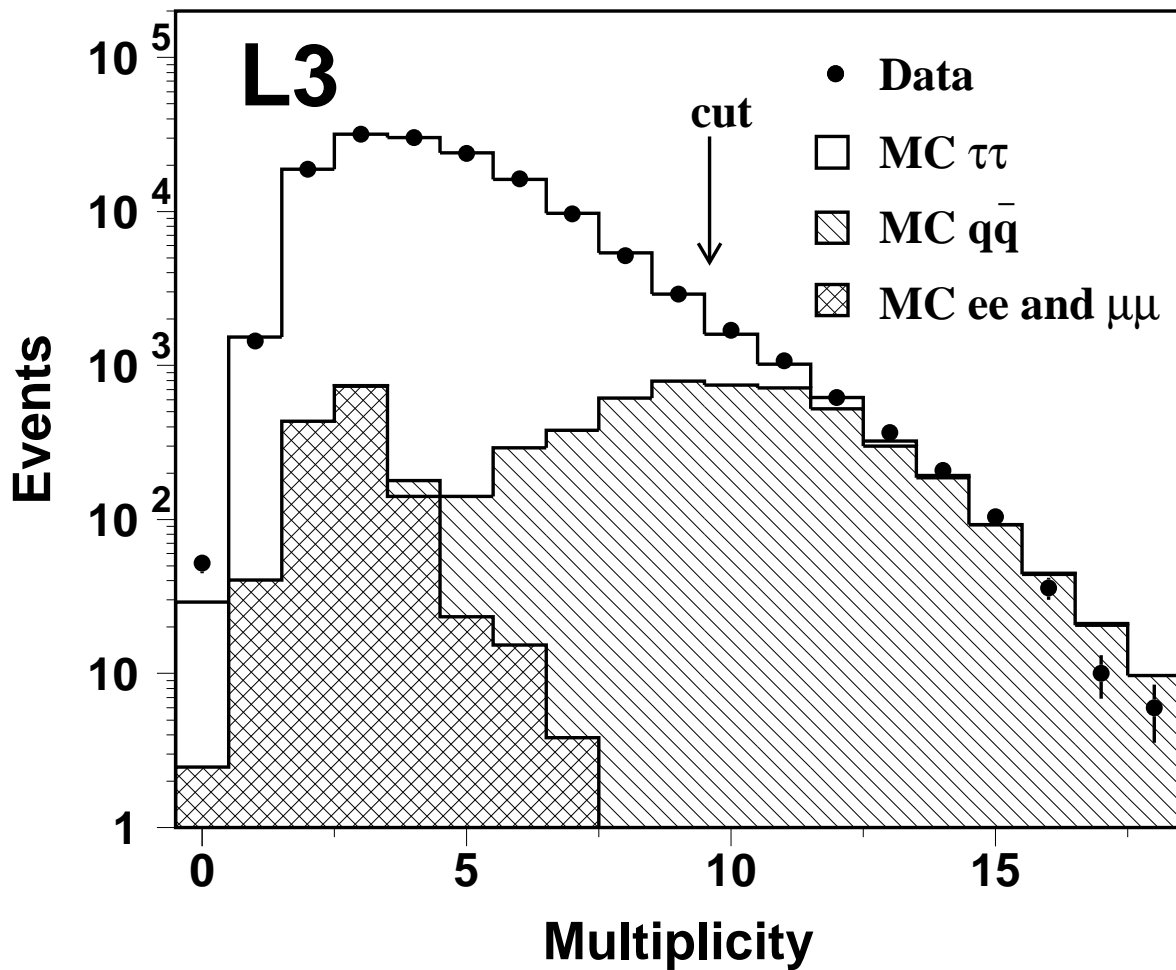


Figure 3: The distribution of the event multiplicity. The Monte Carlo prediction for $e^+e^- \rightarrow \tau^+\tau^-(\gamma)$ and the background from other leptonic and hadronic Z decays after application of the scale factors is also given.

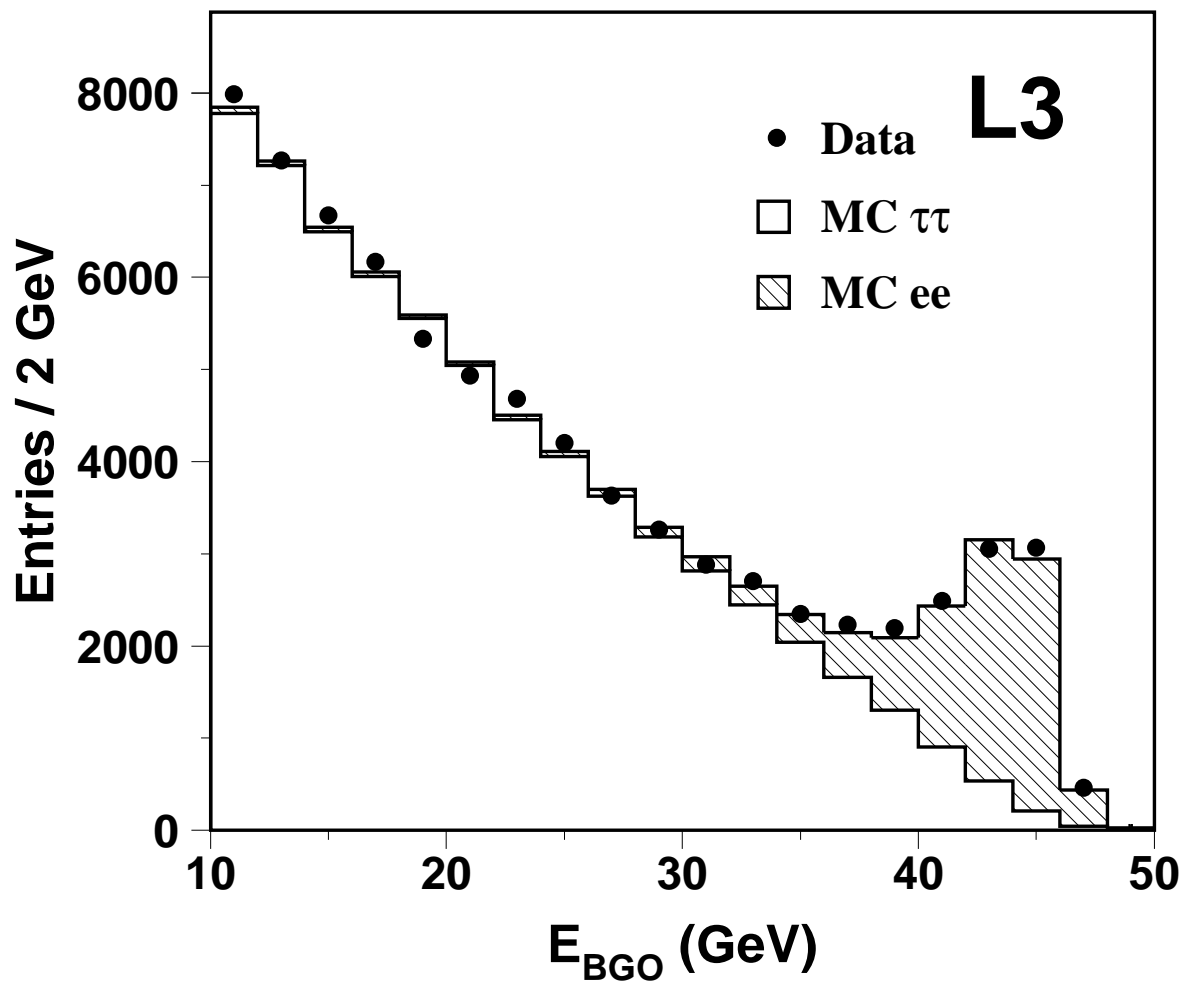


Figure 4: The distribution of the BGO energy for selected $e^+e^- \rightarrow \tau^+\tau^-(\gamma)$ events with relaxed cuts against $e^+e^- \rightarrow e^+e^-(\gamma)$ background. Also shown is the Monte Carlo expectation for $e^+e^- \rightarrow \tau^+\tau^-(\gamma)$ and $e^+e^- \rightarrow e^+e^-(\gamma)$ events after rescaling.

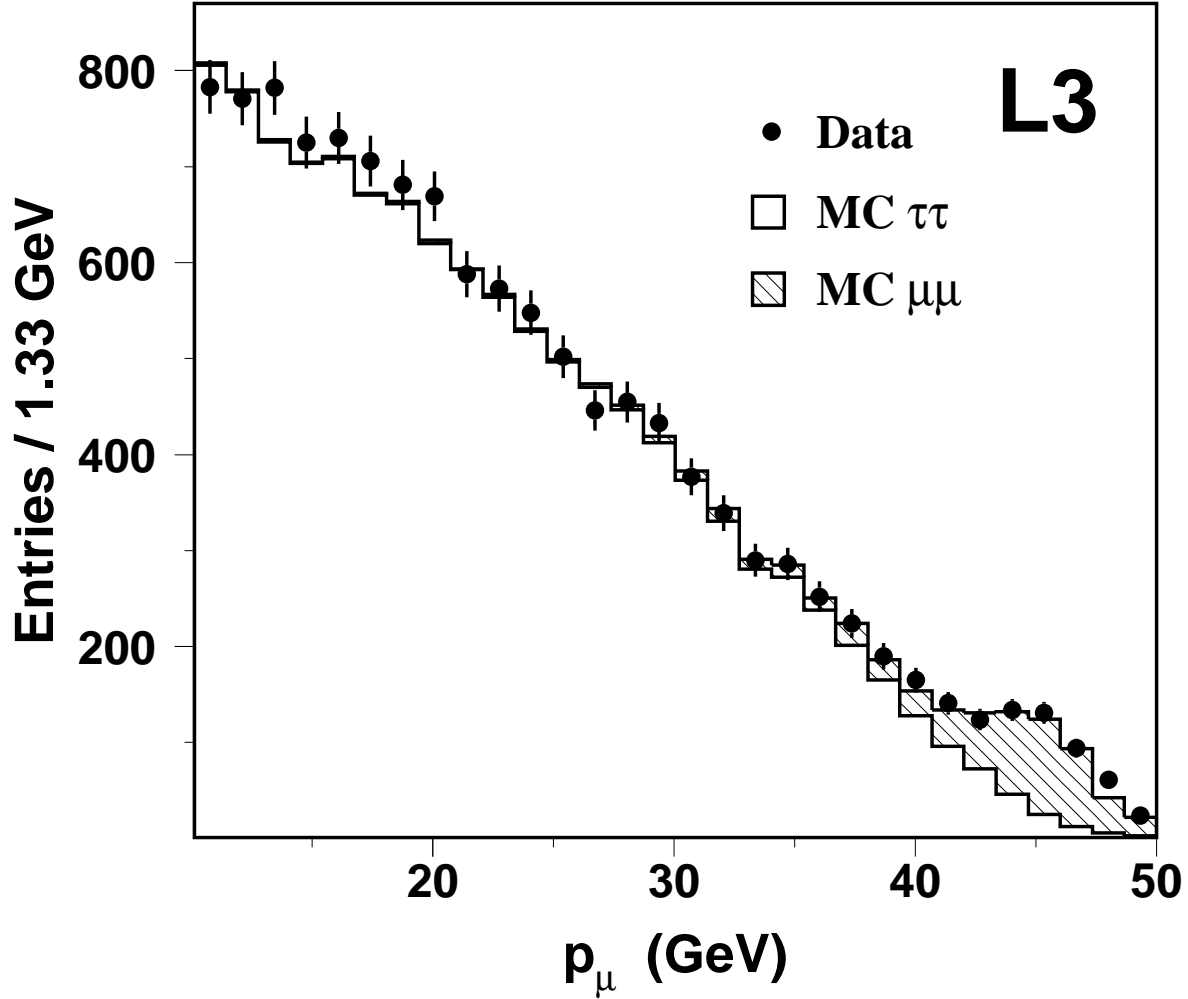


Figure 5: The momentum distribution of tracks measured in the muon chambers in the $e^+e^- \rightarrow \tau^+\tau^-(\gamma)$ event sample with relaxed cuts against dimuon background. Also shown is the Monte Carlo expectation for $e^+e^- \rightarrow \tau^+\tau^-(\gamma)$ and the background from dimuon final states after rescaling.

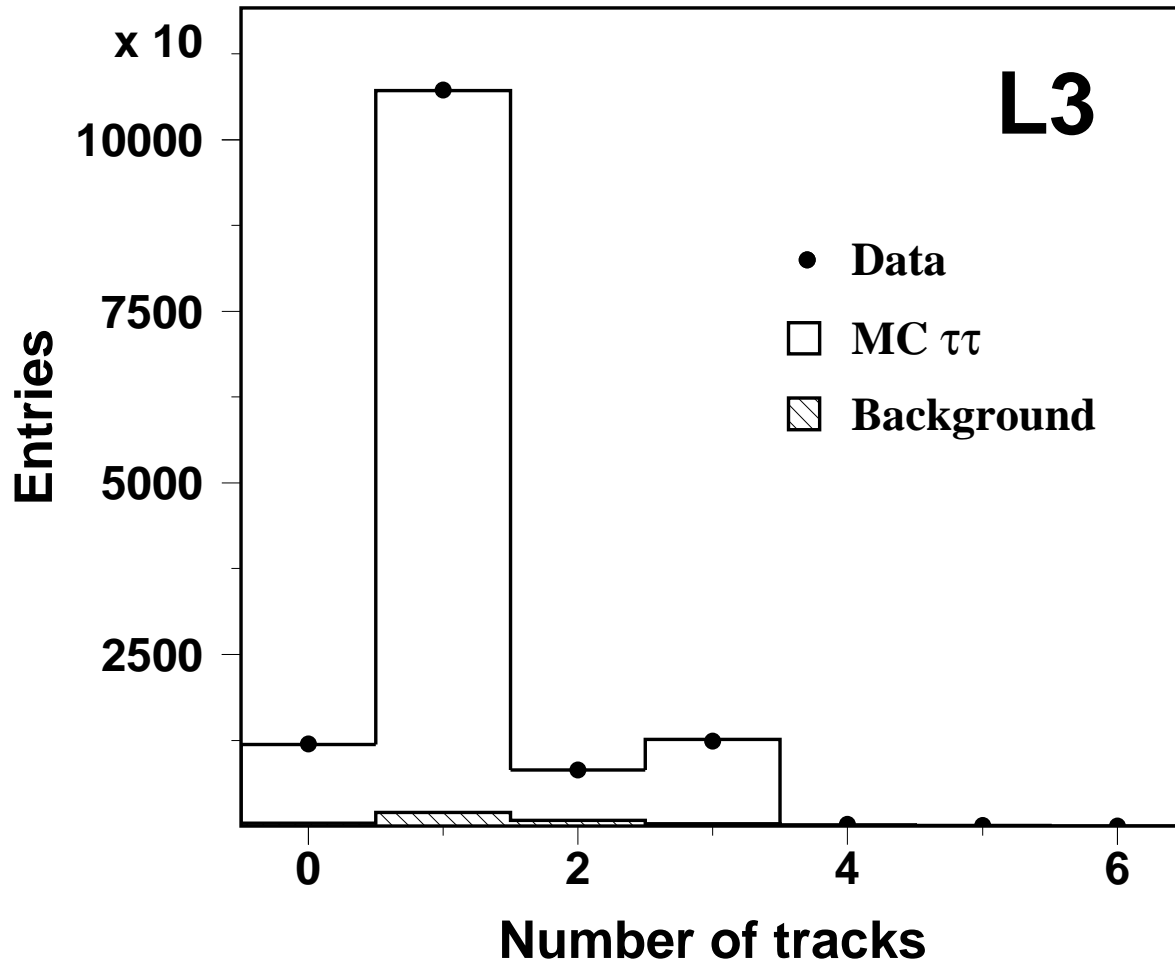


Figure 6: The charged multiplicity distribution from τ decays. Also shown is the expectation from Monte Carlo for $e^+e^- \rightarrow \tau^+\tau^-(\gamma)$ and the background.

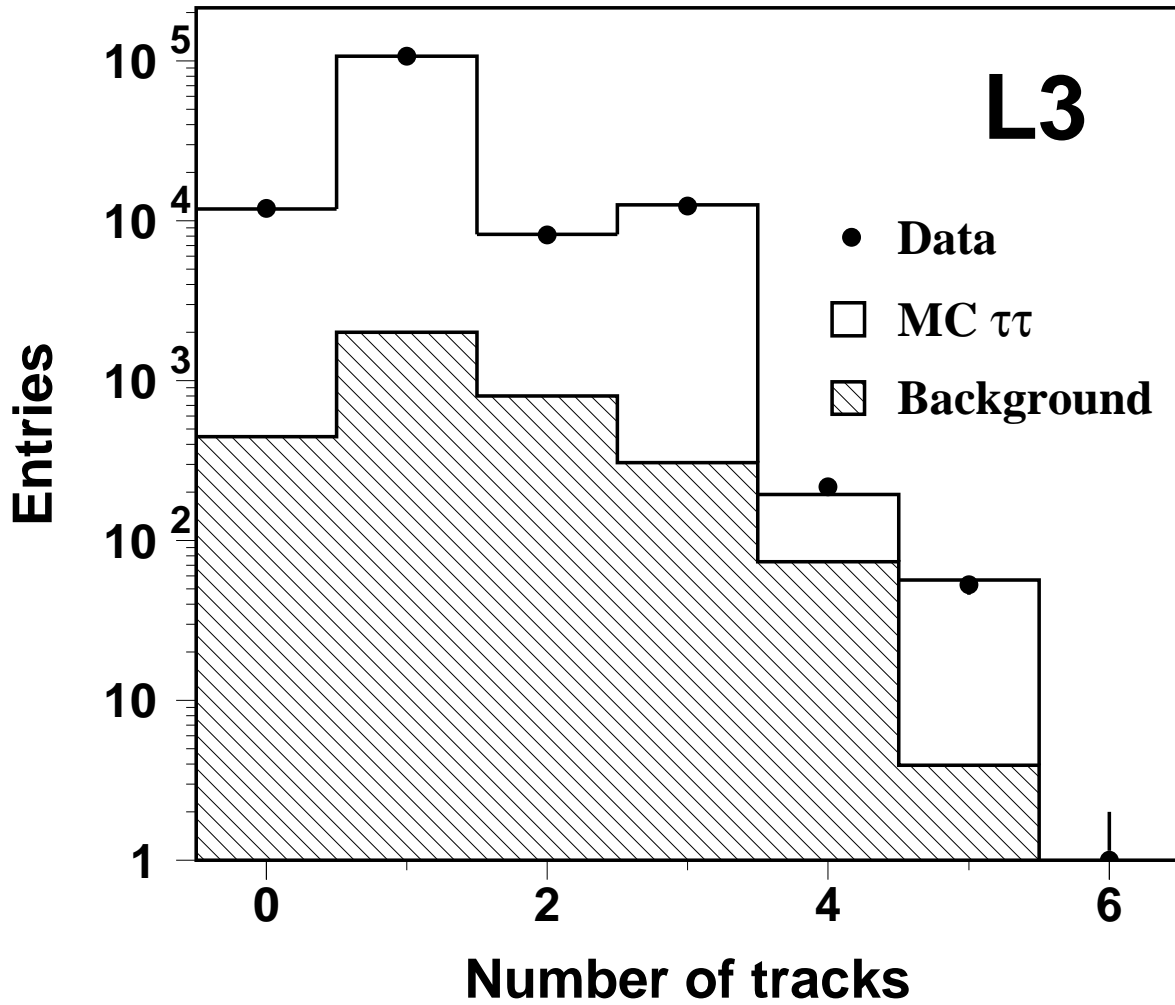


Figure 7: The charged multiplicity distribution from τ decays. Also shown is the expectation from Monte Carlo for $e^+e^- \rightarrow \tau^+\tau^-(\gamma)$ and the background from hadronic Z decays and other sources.